J|A|C|S
ARTICLES
Published on Web 12/12/2007

The Use of Size-Selective Excitation To Study Photocurrent through Junctions Containing Single-Size and Multi-Size Arrays of Colloidal CdSe Quantum Dots

Emily A. Weiss,[‡] Venda J. Porter,[§] Ryan C. Chiechi,[‡] Scott M. Geyer,[§] David C. Bell,[†] Moungi G. Bawendi,*[,§] and George M. Whitesides*[,‡]

Department of Chemistry and Chemical Biology, Harvard University, 12 Oxford Street, Cambridge, Massachusetts 02138, Department of Chemistry, Massachusetts Institute of Technology, 77 Massachusetts Avenue, Cambridge, Massachusetts 02139, and Center for Nanoscale Systems, Harvard University, 11 Oxford Street, LISE 306, Cambridge, Massachusetts 02138

Received September 3, 2007; E-mail: gwhitesides@gmwgroup.harvard.edu; mgb@mit.edu

Abstract: This paper describes a study of the generation and flow of photocurrent through junctions containing three-dimensional arrays of colloidal CdSe quantum dots (QDs) of either a single size or multiple sizes. The electrodes were indium tin oxide (ITO) covered with a thin layer of poly(3,4-ethylenedioxythiophene):poly(styrenesulfonate) (PEDOT:PSS) and a eutectic alloy of Ga and In (EGaIn). We measured the current−voltage characteristics of the junctions in the dark and under illumination, with various sources and wavelengths of excitation, and their photocurrent action spectra. Size-selective photoexcitation of the arrays of multiple sizes of QDs helped to determine (i) the location of the interface at which photoinduced separation of charge occurred, (ii) whether the energy absorbed by the QDs was redistributed before separation of charge, and (iii) the dependence of the photovoltage on the locations of various sizes of QDs within the junction. This research is a step toward the use of QDs for harvesting light and for transporting energy and charge in devices—for example, solar cells and photodetectors—that operate at zero bias.

Introduction

This paper describes a study of the mechanisms by which photoexcitation enhances the flow of current through junctions containing layers of colloidal CdSe quantum dots (QDs) of a single size or stacked layers of QDs of different sizes (Figure 1a).[1] Indium tin oxide (ITO) covered with a thin layer of poly-(3,4-ethylenedioxyl-thiophene):poly(styrene sulfonate) (PEDOT:PSS) supported the QDs, and a eutectic mixture of Ga and In (EGaIn)[2] served as a conformal top-contact. The electronic and optical properties of QDs depend sensitively on their size; incorporation of multiple sizes of QDs organized in layers in a single array therefore provided a means for size-selective (and, in turn, localized) photoexcitation within the array. This approach enabled us to determine (i) the location of the interface at which photoinduced separation of charge (to create mobile electrons and holes from excitons) occurred, (ii) whether the energy absorbed by the QDs was redistributed before separation of charge, and (iii) the dependence of the photovoltage on the locations of various sizes of QDs within the junction. A mechanistic understanding of these issues is required for the effective utilization of semiconductor QDs in solar cells[3] and photodetectors,[4] for which they are attractive materials due to their solution processability, high extinction coefficients, good photostability, tunable absorption spectra,[5,6] and potential for multi-exciton generation.[7,8] The arrays containing multiple sizes of QDs also suggest strategies for improving the efficiency of optoelectronic devices through vectorial transfer of energy and charge.[1]

Nomenclature. We use the letters S, M, and L to designate small ($d = 4.2$ nm), medium ($d = 5.3$ nm), and large ($d = 9.8$ nm) CdSe quantum dots, respectively, and P to indicate a ∼20-nm-thick layer of PEDOT:PSS. For example, the film ITO/P/SML consists of stacked layers (where a "layer" is a multilayer, not a monolayer) of each of the S, M, and L QDs spun, successively, onto the glass/ITO/PEDOT:PSS substrate, and with the layer of small QDs adjacent to the PEDOT:PSS (Figure 1a). The junction ITO/P/SML/EGaIn is an ITO/P/SML film with the layer of large QDs contacting the EGaIn electrode. The shorthand "junction SML" means the junction ITO/P/SML/EGaIn, and ITO/P/L**X**/EGaIn is a junction with L QDs adjacent

[‡] Department of Chemistry and Chemical Biology, Harvard University.
[§] Department of Chemistry, Massachusetts Institute of Technology.
[†] Center for Nanoscale Systems, Harvard University.

(1) Weiss, E. A.; Chiechi, R. C.; Geyer, S. M.; Porter, V. J.; Bell, D. C.; Bawendi, M. G.; Whitesides, G. M. *J. Am. Chem. Soc.* **2007**, ASAP (ja076438h).
(2) Chiechi, R. C.; Weiss, E. A.; Dickey, M. D.; Whitesides, G. M. *Angew. Chem.*, Early View (doi:10.1002/ani.200703642), and references therein.
(3) Huynh, W. U.; Dittmer, J. J.; Alivisatos, A. P. *Science* **2002**, *295*, 2425.
(4) Oertel, D. C.; Bawendi, M. G.; Arango, A. C.; Bulovic, V. *Appl. Phys. Lett.* **2005**, *87*, 213505/1.
(5) Murray, C. B.; Kagan, C. R.; Bawendi, M. G. *Annu. Rev. Mater. Sci.* **2000**, *30*, 545.
(6) Grundmann, M.; Christen, J.; Ledentsov, N. N.; Bohrer, J.; Bimberg, D. *Phys. Rev. Lett.* **1995**, *74*, 4043.
(7) Guyot-Sionnest, P. *Nat. Mater.* **2005**, *4*, 653.
(8) Nozik, A. J. *Physica E* **2002**, *14*, 115.

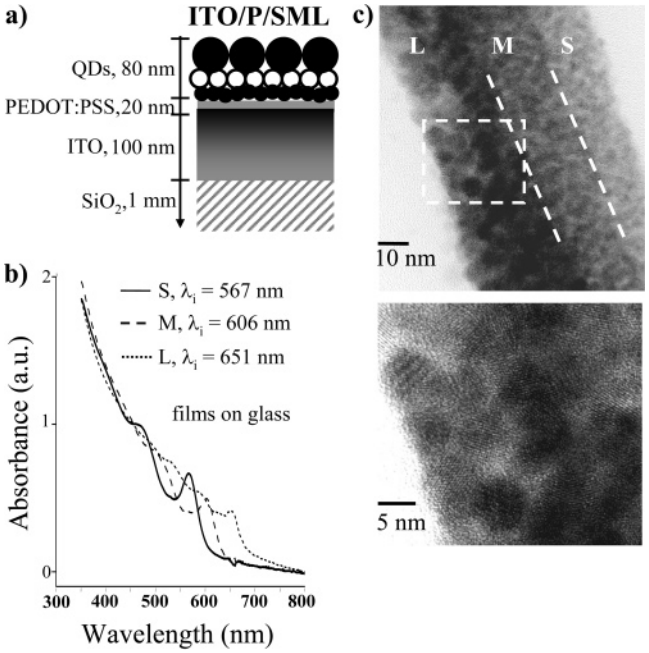

Figure 1. (a**)** Schematic cross section of the film ITO/PEDOT:PSS/SML. The nomenclature is explained in the text. Each row of QDs represents a multilayer that is ∼25 nm thick. (b**)** Ground-state absorption spectra of butylamine-treated films of S (d = 4.2 nm), M (d = 5.3 nm), and L (d = 9.8 nm) QDs spun on glass from solutions in $CHCl_3$ (with concentrations 1×10^{-5} M (L), 6.5×10^{-5} M (M), and 1×10^{-4} M (S)). The symbol λ_i indicates the wavelength of the maximum of the band-edge absorption. This maximum is at lower energy in the spectra of the films than in the spectra of the solutions (Figure S1) due to electronic interactions among the QDs in the film. (c) Top: TEM micrograph of a cross section of the SML QD film spun onto, and subsequently embedded in, epoxy (on a lacey carbon grid). The Supporting Information (Figure S3) contains the procedure for making the TEM sample. The white dotted lines indicate the boundaries between layers of QDs of different size. Bottom: High-resolution TEM image (of the boxed region in the top image) showing the crystal lattice of individual QDs.

to the PEDOT:PSS layer and an unspecified combination of QDs (**X**) in the rest of the array. The notation $EQE(LLL)_{660}$ means the external quantum efficiency (defined later) of the junction LLL when it is illuminated with light that has a wavelength of 660 nm. The symbol V is the bias applied to the junction—that is, the difference in voltage between the ITO and the EGaIn electrodes. When V is positive, EGaIn is biased positively with respect to ITO; when V is negative, EGaIn is biased negatively with respect to ITO.

Experimental Design

Materials. Arrays of CdSe QDs are popular model systems for studying the effect of size on optical and electronic properties, and for exploring the potential of quantum-confined semiconductors as materials for inorganic[8,9] and inorganic−organic hybrid[10] solar cells. Many groups[11−18] now routinely synthesize macroscopic quantities of monodisperse (σ < 4% rms) CdSe QDs at temperatures less than 400 °C using wet-chemical procedures. The QDs have diameters ranging from 12 to 150 Å (the bulk exciton radius of CdSe is ∼50 Å[19]), good electronic passivation, and uniform shape.[11,20,21] Cadmium selenide QDs have a finely tuned profile of absorption vs size with good coverage of the visible spectrum: for d = 12−150 Å, absorption at the band-edge ranges from 2.9 eV (∼425 nm) to 1.75 eV (∼710 nm).[5,11,22−26] The excitation transfer[5,22,26,27] and photoconductivity[28−30] within 3D colloidal glasses and crystals of CdSe QDs is well characterized. Decreased interdot spacing and improved passivation of surface trap sites[31]—through, for example, the treatment with butylamine that we employ here—increases the magnitude of photocurrent by up to a factor of 10^3 from that of untreated films of CdSe QDs.[32,33] Furthermore, since the energies of their HOMOs and LUMOs are lower than those of many hole-transporting, light-absorbing conjugated polymers, the QDs can either accept electrons or donate holes to these polymers; this energetic alignment makes the combination of CdSe QDs and conducting organic polymers an attractive choice for electro-optic devices that are composites of multiple materials.[34,35]

Studies of junctions incorporating ITO are relevant to the development of a wide range of devices: ITO is the most commonly used transparent conducting oxide for electrodes for organic and dye-sensitized photovoltaics, light-emitting diodes, electrochromics, electroluminescent devices, displays, and heat-reflective coatings.[36] Indium tin oxide is often coupled with the polymeric hole-conductor PEDOT:PSS, which, conveniently, may be spin-coated from commercially available aqueous suspensions. This polymer is effectively transparent throughout the long-wavelength UV and visible regions of the spectrum and provides a smooth, conformal contact between the active material (here, QDs) and the rough, hydrophilic surface of ITO; this contact improves the kinetics of collection of charge.[37,38]

Using the procedures we describe here and the conformal EGaIn electrode, we were able to produce large numbers of junctions in nearly

(9) Klimov, V. I. *Appl. Phys. Lett.* **2006**, *89*, 123118/1.
(10) Gur, I.; Fromer, N. A.; Alivisatos, A. P. *J. Phys. Chem. B* **2006**, *110*, 25543.
(11) Murray, C. B.; Norris, D. J.; Bawendi, M. G. *J. Am. Chem. Soc.* **1993**, *115*, 8706.
(12) Snee, P. T.; Chan, Y.; Nocera, D. G.; Bawendi, M. G. *Adv. Mater.* **2005**, *17*, 1131.
(13) Boatman, E.; Lisensky, G. C.; Nordell, K. J. *J. Chem. Educ.* **2005**, *82*, 1697.
(14) Li, J. J.; Wang, Y. A.; Guo, W.; Keay, J. C.; Mishima, T. D.; Johnson, M. B.; Peng, X. *J. Am. Chem. Soc.* **2003**, *125*, 12567.
(15) Peng, X.; Wickham, J.; Alivisatos, A. P. *J. Am. Chem. Soc.* **1998**, *120*, 5343.
(16) Shim, M.; Wang, C.; Guyot-Sionnest, P. *J. Phys. Chem.* **2001**, *105*, 2369.
(17) Talapin, D. V.; Schevchenko, E. V.; Kornowski, A.; Gaponik, N.; Haase, M.; Rogach, A. L.; Weller, H. *Adv. Mater.* **2001**, *13*, 1868.
(18) Munro, A. M.; Plante, I. J.-L.; Ng, M. S.; Ginger, D. S. *J. Phys. Chem. C* **2007**, *111*, 6220.
(19) Kittel, C. *Introduction to Solid State Physics*, 7th ed.; John Wiley and Sons: New York, 1996
(20) Bowen Katari, J. E.; Colvin, V. L.; Alivisatos, A. P. *J. Phys. Chem.* **1994**, *98*, 4109.
(21) Peng, Z. A.; Peng, X. *J. Am. Chem. Soc.* **2001**, *123*, 183.
(22) Kagan, C. R. Basic Physics of Semiconductor Quantum Dots; Proceedings of the NSF−Conicet Quilmes Nanoscience Workshop 2003, Quilmes, Provincia de Tucuman, Argentina.
(23) Norris, D. J.; Bawendi, M. G.; Brus, L. E. Optical Properties of Semiconductor Nanocrystals. In *Molecular Electronics*; Jortner, J., Ratner, M. A., Eds.; Blackwell Science Ltd.: Malden, MA, 1997; p 281.
(24) Greenham, N. C.; Peng, X.; Alivisatos, A. P. *Phys. Rev. B* **1996**, *54*, 17628.
(25) Landsberg, P. T.; Nussbaumer, H.; Willeke, G. *J. Appl. Phys.* **1993**, *74*, 1451.
(26) Kagan, C. R.; Murray, C. B.; Bawendi, M. G. *Phys. Rev. B* **1996**, *54*, 8633.
(27) Kagan, C. R.; Murray, C. B.; Nirmal, M.; Bawendi, M. G. *Phys. Rev. Lett.* **1996**, *76*, 1517.
(28) Leatherdale, C. A.; Kagan, C. R.; Morgan, N. Y.; Empedocles, S. A.; Kastner, M. A.; Bawendi, M. G. *Phys. Rev. B* **2000**, *62*, 2669.
(29) Ginger, D. S.; Greenham, N. C. *J. Appl. Phys.* **2000**, *87*, 1361.
(30) Morgan, N. Y.; Leatherdale, C. A.; Drndic, M.; Jarosz, M. V.; Kastner, M. A.; Bawendi, M. G. *Phys. Rev. B* **2002**, *66*, 075339.
(31) Yen, B. K. H.; Stott, N. E.; Jensen, K. F.; Bawendi, M. G. *Adv. Mater.* **2003**, *15*, 1858.
(32) Jarosz, M. V.; Porter, V. J.; Fisher, B. R.; Kastner, M. A.; Bawendi, M. G. *Phys. Rev. B* **2004**, *70*, 195327/1.
(33) Porter, V. J.; Mentzel, T.; Charpentier, S.; Kastner, M. A.; Bawendi, M. G. *Phys. Rev. B* **2006**, *73*, 155303/1.
(34) The electron affinity (EA) of CdSe is 4.87 eV in bulk and, within the effective mass approximation, is ∼4.4 eV for an QD with d = 3.5 nm, so it acts as an electron acceptor to the excited states of both poly[2-methoxy-5-(2′-ethylhexyloxy)-1,4-phenylene vinylene] (MEH-PPV), and poly(3-hexylthiophene) (P3HT), which are commonly used as hole-conducting layers in heterojunction PV cells.
(35) Qi, D.; Fischbein, M.; Drndic, M.; Selmic, S. *Appl. Phys. Lett.* **2005**, *86*, 093103.
(36) Cui, J.; Wang, A.; Edleman, N. L.; Ni, J.; Lee, P.; Armstrong, N. R.; Marks, T. J. *Adv. Mater.* **2001**, *13*, 1476.
(37) Kushto, G. P.; Kim, W.; Kafafi, Z. H. *Appl. Phys. Lett.* **2005**, *86*, 093502.
(38) Ouyang, J.; Chu, C.-W.; Chen, F.-C.; Xu, Q.; Yang, Y. *Adv. Funct. Mater.* **2005**, *15*, 203.

100% yield—where yield is the fraction of junctions that did not short as a result of contact between the ITO or the PEDOT:PSS and the EGaIn through defects in the film of QDs.[1,2] The non-Newtonian properties of EGaIn—that is, its tendency to flow like a liquid under shear stress but hold its shape once this stress falls below a characteristic threshold value (~100 Pa)—allow it (following procedures described elsewhere[2]) to form small (micrometers to hundreds of micrometers in diameter) conformal contacts. Unlike the evaporation of a top-contact of a solid metal (typically gold), the fabrication of solid−EGaIn junctions does not damage the organic ligands on the QDs or form persistent metal filaments that may short the junction or cause artificially high currents. Eutectic Ga/In is particularly suited as an electrode for use with CdSe QDs because its Fermi level (E_F) (which we assume to be some value between that of In, $E_F(\text{In}) = -4.1$ eV, and that of Ga, $E_F(\text{Ga}) = -4.2$ eV)[39] is close to the energies of their LUMOs. Eutectic Ga/In can therefore easily exchange electrons with the QDs, unlike Au ($E_F \approx -5.3$ eV), which makes a so-called "blocking contact" [29,32,33] with many types of semiconductor QDs.

Arrays of QDs of Multiple Sizes. A study of photoinduced charge transport through a series of junctions, each containing an array of a single size of QDs, yields, in principle, the dependence of the electrical characteristics of the junctions on the size of the QDs. The incorporation of arrays of multiple sizes of QDs into the junction allows us to separate the observed dependence of current density (J) on the bias (V) applied to the junction and on photoexcitation of the QDs into contributions from transport across the interfaces between QDs and the electrodes and transport through the array: When multiple sizes of QDs with distinct band-edge absorptions are present within a single junction, we can achieve spatial selectivity of photoexcitation—that is, we can choose to excite only the QDs near the PEDOT:PSS, only the QDs near the EGaIn, or the entire array. This strategy makes it possible to determine the relationship between the location of a QD within the junction and its contribution to the observed photocurrent. Furthermore, once the interface for separation of charge is identified, an architecture for the junction based on multiple sizes of QDs has the potential to allow funneling of absorbed light to that interface through an energy-transfer process that is energetically "downhill"; this type of "cascaded energy-transfer structure" has been realized in arrays of CdTe nanocrystals by Franzl et al.[40]

Results and Discussion

Preparation of Films of QDs on ITO/PEDOT:PSS. The solution-phase synthesis of CdSe QDs has been published previously;[12] we give details in the Supporting Information. We used this synthesis to generate three sizes of nanocrystals, whose band-edge absorptions have maxima at $\lambda_i = 560$ nm (small QDs, S), 604 nm (medium QDs, M), and 650 nm (large QDs, L), as characterized by ground-state absorption in solution in hexanes (Figure S1). We used trioctylphosphine oxide (TOPO) as an organic capping layer for all of the QDs in suspension. Following previous methods for making films containing close-packed QDs,[11,22,28,32,33,41] we precipitated the QDs from a suspension in methanol three times.

The films of QDs were vertical stacks of layers of CdSe QDs of a given diameter (Figure 1). We studied five different types of films of QDs: ITO/P/**X**, **X** = LLL, MMM, SSS, SML, or LMS. We began by spin-coating PEDOT:PSS (Baytron-P) from a 2:1 dilution of the commercially available aqueous suspension (Bayer, conductive grade) in deionized water at 5000 rpm for 1 min onto ITO (on float glass, Delta Technologies, $R = 8-12$ Ω/square) that had been cleaned with ethanol and dried in a stream of N_2. The PEDOT:PSS film was annealed in a vacuum oven at 120 °C for 30 min. Atomic force microscopy (AFM, Figure S2a) showed that the root-mean-square (rms) roughness of bare ITO was 5.6 nm, and the rms roughness of ITO-P (for a 20 nm-thick layer of PEDOT:PSS) was 4.1 nm, both over an area of 25 μm^2. We then spin-coated the QDs, one layer at a time, at 5000 rpm for 1 min from solutions of $CHCl_3$ in the following concentrations: 1×10^{-5} M (L), 6.5×10^{-5} M (M), and 1×10^{-4} M (S) (determined by measuring the absorbance, at 350 nm, of a set of films spun with different concentrations of solution and constructing a calibration curve). This combination of concentrations and spinning conditions yielded layers that were ~26−29 nm each (Figure S2b), as measured by AFM. After the deposition of each sheet, we soaked the film in a 0.1 M solution of butylamine in acetonitrile to replace the TOPO with butylamine as ligands for the QDs.[32] We then annealed the film at 70 °C for 1 h to drive off any excess (unbonded) organic material and to reorganize the butylamine ligands into their closest-packed, intercalated configuration (~0.2-nm separation between the QDs, as determined by glancing angle X-ray scattering).[32] Figure 1b shows ground-state absorbance spectra of the butylamine-treated films, in which λ_i (the wavelength of the peak of the band-edge absorption) is slightly higher than its value in solution (Figure S1) for each of the sizes of QDs. The bathochromic shift of the peaks in the absorption spectra reflects an increase in the degree of delocalization of the excitonic wavefunction on going from solution to solid-state array.

Figure 1c shows a high-resolution transmission electron microscopy (HRTEM) image of a cross section of the film with three layers, each with a different size of QDs, that was spun onto a slab of thermally cured epoxy (Araldite 502, Electron Microscopy Sciences), sectioned using an ultramicrotome, and imaged on a lacey carbon grid (for details, see another publication[1] and the Supporting Information). The image clearly shows three distinct layers of QDs of different sizes. The layer of small QDs is thinner than 25 nm, probably because the QDs did not wet the epoxy as well as they wet the PEDOT:PSS or the ITO, and the spinning conditions were not adjusted accordingly. We also note that the L QDs appear to be ~7.5 nm in diameter rather than the 9.8 nm obtained from solution-phase absorption measurements. There are several sources of error in estimating the diameter of the QDs from this particular TEM image that would possibly combine to account for this discrepancy: (i) The QDs that we imaged most clearly were those at the edge of the sample (where the cross section was thinnest), but any portion of those QDs that was embedded in the epoxy medium (which includes the QDs near the edge of the sample) are effectively invisible using this technique, so the QDs appear smaller than they actually are. (ii) There is some distortion of the image due to the fact that we probed a multilayer cross section, not a monolayer (as is usually used to estimate the size of QDs). (iii) There is a 1−3% error expected in the size of the scale bar.

Formation of the ITO/P/QD/EGaIn Junctions. In order to record current−voltage ($I-V$) traces while illuminating the sample, we constructed an electrode in which EGaIn (99.99+%, used as-received) filled the hole in a donut-shaped disk made

(39) Sze, S. M. *Physics of Semiconductor Devices*, 2nd ed.; John Wiley and Sons: New York, 1981.
(40) Franzl, T.; Klar, T. A.; Schietinger, S.; Rogach, A. L.; Feldmann, J. *Nano Lett.* **2004**, *4*, 1599.
(41) Murray, C. B.; Kagan, C. R.; Bawendi, M. G. *Science* **1995**, *270*, 1335.

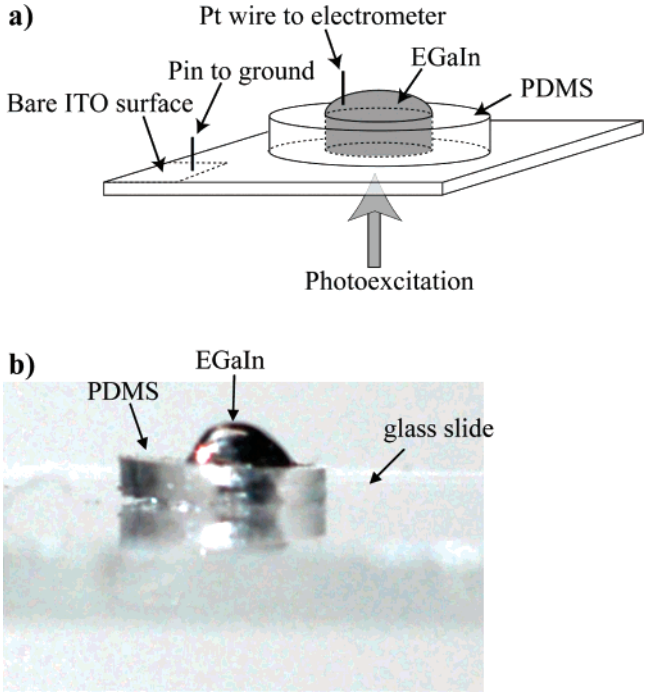

Figure 2. (a) Schematic diagram of the EGaIn junction used for photocurrent experiments: a pin that connects to ground contacts the bare ITO portion of the sample, and the drop of EGaIn that protrudes from the PDMS mold embeds a Pt wire that connects to the electrometer. This drop also contacts the QD film. During the experiment, the sample is suspended by a sample holder perpendicular to the excitation beam. When the excitation source is the Fluorolog or the Ar laser, a lens focuses the beam down to the area of the sample that contacts the EGaIn (diameter = 1 mm, area = 0.008 cm^2). When the excitation source is an LED, the sample is at a distance of 4 cm from the LED, which emits light with a diffusivity characteristic of the LED (see Supporting Information). (b) Photograph of a PDMS mold filled with EGaIn on a glass slide. The EGaIn/PDMS electrode remains adhered to the glass slide (or to a sample) by conformal contact, even when the slide is tilted by 90°. The Supporting Information contains the procedure for making these electrodes.

of cured poly(dimethylsiloxane) (PDMS, Sylgard 184 Silicone) (Figure 2a; see Supporting Information for the procedure for constructing these electrodes). The PDMS and EGaIn portions of this electrode adhered conformally to the layer of QDs on the ITO/PEDOT:PSS substrate such that the entire junction could be mounted with the ITO side of the sample facing the excitation source (Figure 2a,b). The size of the circular junction (diameter = 1 mm, area = 0.008 cm^2) was constant from sample to sample and equaled the size of the hole (cut into the PDMS disk using a biopsy knife). A Pt wire (which was clipped to a cable that went to the electrometer) contacted the EGaIn that protruded from the PDMS, and a pin in the sample holder (connected to ground) contacted a square of exposed ITO on the sample to complete the circuit. Electrons flowed from ITO to EGaIn when the EGaIn was biased positively with respect to the ITO ($V > 0$), and from EGaIn to ITO when the EGaIn was biased negatively with respect to the ITO ($V < 0$).[42]

Electronic Structure of the Junctions. Figure 3 shows a simplified electronic-structure diagram of the components of the ITO/P/QD/EGaIn junction; we will use this diagram to discuss the observed electrical characteristics of the junction. The diagram summarizes the energy levels of the highest occupied molecular orbital (HOMO) and lowest unoccupied molecular orbital (LUMO) for each size of QD, the Fermi levels of ITO[43] and EGaIn,[39] and the conduction band (CB) and valence band (VB) of PEDOT:PSS *before* thermal equilibration of the junction (which is discussed in the Proposed Mechanism for Generation of Photocurrent section, below).

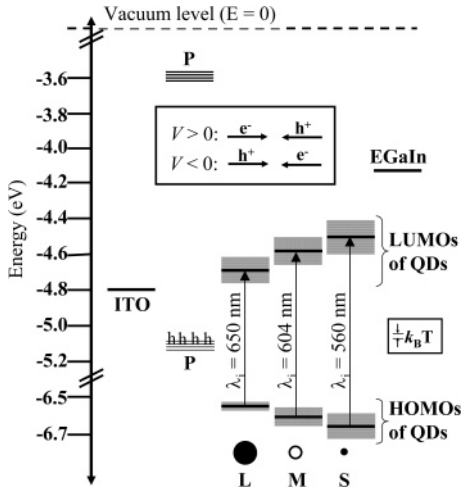

Figure 3. Energy diagram for the individual components of the ITO/P/QD/EGaIn junctions: the Fermi level of ITO (before thermal equilibration with EGaIn), the valence and conduction bands of PEDOT:PSS, the HOMOs and LUMOs of the S, M, and L dots (calculated as explained in the text), and the Fermi level of EGaIn (before thermal equilibration with ITO). The gray boxes indicate the uncertainty in the energies of the HOMOs and LUMOs of the QDs (also explained in the text). The arrows indicate the direction that the electrons move when $V < 0$, where the device turns on, and when $V > 0$, where there is only leakage current in the dark but photocurrent under illumination. The symbol "h" in the VB of PEDOT:PSS indicates the presence of uncharged (counterion-stabilized) holes.

It has not been determined definitively whether the HOMO and LUMO of a CdSe QD split symmetrically or asymmetrically from the energies of the VB and CB, respectively, of bulk CdSe as the size of the QD decreases and its band gap, E_g, increases. The argument for an asymmetric splitting is that, in CdSe, the effective mass of the electron is significantly smaller than the effective mass of the hole ($m_e = 0.13m_o$, $m_h = 1.14m_o$, where m_o is the mass of a free electron);[44] according to the effective mass approximation (EMA),[44] most of the increase in band gap (specifically, ~75% of the increase) from larger QDs to smaller QDs therefore should appear as a shift in their LUMOs. The results of more sophisticated theoretical methods have brought the usefulness of the EMA for predicting the electronic structure of semiconductor QDs into question[45,46] and have suggested a symmetric splitting of energy levels (or at least more symmetric than that given by the EMA); a symmetric splitting gives E_{HOMO}-(QD) = E_{VB}(bulk CdSe) − (E_g(QD) − E_g(bulk CdSe))/2, and E_{LUMO}(QD) = E_{CB}(bulk CdSe) + (E_g(QD) − E_g(bulk CdSe))/2. The difference between the results obtained from the symmetric splitting and those obtained from the asymmetric splitting is minimal (0.1 eV or less), and the set of qualitative conclusions that we draw in this work would hold true no matter which we chose; nonetheless, for the sake of completeness, the energies of the HOMOs and LUMOs of the QDs in Figure 3 are an average of the energies obtained from these two methods.

(42) The direction of flow of electrons is formally opposite that of current, so, at $V > 0$, the current flows from EGaIn through the QDs to ITO, and at $V < 0$, the current flows from ITO through the QDs to EGaIn.

(43) Ishii, H.; Sugiyama, K.; Ito, E.; Seki, K. *Adv. Mater.* **1999**, *11*, 605.
(44) Norris, D. J.; Bawendi, M. G. *Phys. Rev. B* **1996**, *53*, 16338.
(45) Franceschetti, A.; Zunger, A. *Phys. Rev. Lett.* **1997**, *78*, 915.
(46) He, L.; Bester, G.; Zunger, A. *Phys. Rev. Lett.* **2005**, *95*, 246804.

The energy calculated assuming an asymmetric splitting dictates the upper bound of the uncertainty in the energy of the HOMO (top of the gray box); the energy calculated assuming a symmetric splitting dictates the lower bound of the uncertainty in the energy of the HOMO (bottom of the gray box). The uncertainty in the energies of the LUMOs of the QDs is the full width at half-maximum of the band-edge absorption peaks that yielded E_g; this width is larger than the difference between the energies calculated from the two methods.

Excitation of the QDs Produces Photocurrent through the Junctions. We have shown elsewhere[1] that, in the dark, the ITO/PEDOT:PSS/QD/EGaIn junctions are diodes: they turn "on" (there is net electron transport from the EGaIn to the ITO) when V is negative but pass only a small leakage current (where there is net electron transport from the ITO to the EGaIn) when V is positive. Here, we observed that photoexcitation with light that has a frequency resonant with, or of higher energy than, the absorption of the QDs produced photocurrent ($I_{light} - I_{dark}$) in the junction when $V = 0$ or $V > 0$.[47]

Figure 4a shows the values of the current (I) measured when we scanned V from $0 \rightarrow +1.0\ V \rightarrow 0$ (in steps of 0.1 V) for the junction SSS in the dark, and when the sample was illuminated with light at 565 and 660 nm. We allowed the junction to equilibrate at the specified V for 1 s before recording the current. Each point in the plot in Figure 4a is the log-mean ($\langle I \rangle_{log}$) of 14 values of I (where $\langle I \rangle_{log} = 10^{\langle \log I \rangle}$, and $\langle \log I \rangle$ is the mean value of $\log(|I|)$) measured over five separate junctions.[48] This plot is meant to demonstrate the presence of a photo-effect; the error for the magnitude of this effect in all of the junctions is in Figure 4b, which is discussed in the next paragraph. The sources of excitation used to gather the data in Figure 4a were light-emitting diodes (LEDs) that were positioned 4 cm from the glass substrate and that illuminated the sample as shown in Figure 2b (see the Supporting Information for the LED specifications). The trace measured with excitation at 660 nm (which the S QDs did not absorb, see Figure 1b) is effectively indistinguishable from the trace measured in the dark, while the current increased by $\sim 10^3$ with excitation at 565 nm (which the S QDs did absorb). This result indicates that, as observed previously,[28] current created upon illumination (photocurrent) was not simply a local heating effect, nor was it a result of thermal or photoexcitation of other materials (besides the QDs) within the device.

External Quantum Efficiencies of the Junctions. Table 1 and Figure 4b give the external quantum efficiencies (EQEs) for the junctions ITO/P/**X**/EgGaIn, **X** = LLL, MMM, SSS, LMS, and SML, when excited by LEDs at 565 and 660 nm. External quantum efficiency is defined as the number of electrons that enter the external circuit per photon incident upon the junction (*not* per photon absorbed by the junction) (eq 1). In eq 1, x is the density of photons incident on the junction (9.80×10^{13} photons s^{-1} cm^{-2} for 565 nm or 1.30×10^{14} photons s^{-1} cm^{-2} for 660 nm), and J_{dark} (J_{light}) (where $J = \langle J \rangle_{log}$,

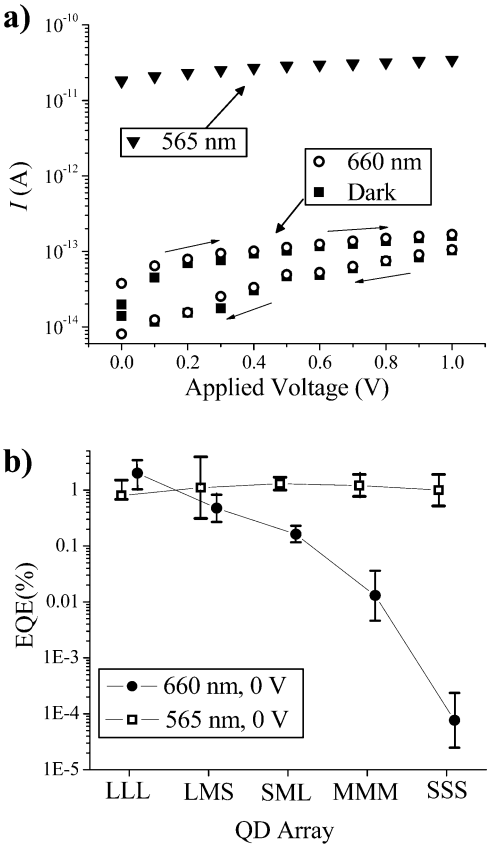

Figure 4. (a) Current−voltage ($I-V$) plots for the junction ITO/P/SSS/EGaIn in the dark (■) and with excitation (using LEDs) at 565 nm (▲) and 660 nm (○). The traces for the data taken in the dark and under illumination at 660 nm were hysteretic; the arrows show the direction in which we scanned V. (b) Plots of the external quantum efficiency (EQE, values are also listed in Table 1), defined as electrons that enter the external circuit per incident photon, at $V = 0$ V for ITO/P/**X**/EGaIn, **X** = LLL, LMS, MMM, SML, and SSS, with excitation (using LEDs) at 565 and 660 nm. The points for each array are offset along the x-axis for clarity. The lines connecting data obtained at a common wavelength are to guide the eye. The text contains the equation used to calculate EQE for our system, and the Supporting Information describes the calculation of the error bars.

$$\mathrm{EQE} = (J_{light} - J_{dark})[(1.6 \times 10^{-19} C)(x)]^{-1} \qquad (1)$$

as defined above) is the current density through the junction in the dark (under illumination) at $V = 0$ V. The values in Table 1 are EQE(%), which is EQE × 100. In general, the EQE is determined by the amount of light the array of QDs absorbs at the wavelength of excitation, the number of resulting excitons that separate into charge carriers (electrons and holes), and the efficiency of the collection of charge. We determined the density of incident photons by shining the light from the LED on a silicon detector of known photo-responsivity and area (the LED was positioned 4 cm from the detector, as with the QD samples). In order to calculate the number of incident photons, we integrated this density over the area of the EGaIn junction defined by the PDMS mold (diameter = 1 mm, area = 0.008 cm^2).

The ranges for each EQE in Table 1, and the error bars in Figure 4b, reflect the error in the EQE propagated from the uncertainty in the photocurrent (using between 14 and 21 measurements for each array at each value of V; the Supporting Information contains the complete error analysis). Even with this large error, Table 1 and Figure 4b show that, as expected from inspection of Figure 4a and the absorption spectrum of

(47) We also saw up to a 100-fold (but usually less than 10-fold) increase in current upon photoexcitation when the EGaIn was biased negatively with respect to the ITO (i.e., under forward bias), but this enhancement is probably due to (i) creation of charge carriers from quantum-confined photoexcited states in the QD layers and (ii) filling of cationic surface traps on the QDs.

(48) We have used the log-mean, rather than the arithmetic mean ($\langle I \rangle$), because the values for $\log(I)$ fit a normal distribution better than did the values for I.

Table 1. External Quantum Efficiency (EQE) of the Junctions ITP/P/**X**/EGaIn under Illumination (with Excitation from LEDs at 565 and 660 nm) at Selected Volatages

	EQE (%)[a]			
	0 V		+0.5 V	
X	565 nm	660 nm	565 nm	660 nm
LLL	**0.80**, 0.71−1.5	**3.8**, 1.9−6.7	**2.1**, 1.4−3.2	**7.9**, 3.9−14.0
LMS	**1.1**, 0.31−3.9	**0.84**, 0.46−1.5	**2.3**, 0.87−6.1	**1.8**, 0.59−5.5
MMM	**1.2**, 0.77−1.9	**0.019**, 0.0064−0.056	**1.5**, 0.99−2.3	**0.21**, 0.081−0.54
SML	**1.3**, 1.0−1.7	**0.27**, 0.19−0.39	**1.7**, 1.3−2.2	**0.49**, 0.39−0.61
SSS	**1.0**, 0.52−1.9	$\mathbf{8.5\times10^{-5}}$, 2.6×10^{-5}−2.8×10^{-4}	**1.6**, 0.70−3.6	$\mathbf{5.8\times10^{-5}}$, 2.5×10^{-5}−1.4×10^{-4}

[a] The EQE (%) is presented as an average (in bold) and a range (see the Supporting Information for error analysis). Equation 1 (in the text) defines EQE.

the S QDs (Figure 1b), $EQE(SSS)_{660}$ is effectively zero. Furthermore, $EQE(MMM)_{660}$ is approximately a factor of 10^2 smaller than $EQE(MMM)_{565}$ at $V = 0$, and approximately a factor of 10 smaller than $EQE(MMM)_{565}$ at $V = 0.5$ V. We did not expect that $EQE(MMM)_{660}$ would be as small as $EQE(SSS)_{660}$, because the "660-nm" LED still emits at half its maximum intensity at 640 nm (see Supporting Information), so the emission spectrum of the LED and the absorption spectrum of the M QDs in the film (Figure 1b) do overlap. These results re-emphasize that the photocurrent originates from excitations of the QDs, since electrons are not produced from photons that have energies below that of the optical band gap (E_g) of the QDs.

Size-Selective Photoexcitation of the QDs Shows That Photocurrent Originates from Separation of Charge at the Interface between the QDs and PEDOT:PSS. We observe that $EQE(SML)_{565}$ is approximately a factor of 5 larger than $EQE(SML)_{660}$ at $V = 0$, and more than a factor of 3 larger than $EQE(SML)_{660}$ at $V = 0.5$ V; $EQE(LMS)_{565} \approx EQE(LMS)_{660}$ at $V = 0$ and 0.5 V (Table 1 and Figure 4b). We can assume that the mobility of charges through the arrays SML and LMS is similar, since they have the same percentage of each size of QD. These arrays also have indistinguishable absorption coefficients at the two wavelengths we used, 565 and 660 nm (Figure S4). The difference in their EQEs must therefore come from a difference in their yields of charge carriers from excitons (their "charge separation efficiency") due to the fact that excitation at 660 nm in these two junctions is "size selective" (i.e., localized): In SML, the excitons created by 660-nm photons are in the L QDs (and somewhat in the M QDs) and are trapped away from the interface with PEDOT:PSS because they have an energy less than E_g of the S QDs.[5] In LMS, the excitons created by 660-nm photons are also trapped in the L QDs, but they are trapped at or near the interface with PEDOT:PSS. Selective excitation of the L QDs thereby reveals that it is only the excitons created at the interface with PEDOT:PSS (or that travel to this interface via energy transfer[27])—and not those trapped at the interface with EGaIn or in the bulk of the QD array—that contribute to the photocurrent. The event that creates electrons and holes from the excitons therefore occurs at the interface between the QDs and PEDOT:PSS.

To confirm this observation, we recorded the $I-V$ curves for the junctions LMS and SML in the dark, and when photoexcited at 647 nm, with a continuous-wave (CW) Ar-ion laser, which has a narrower bandwidth (a small fraction of a nm) and a higher power (intensity of 10 mW/cm^2) than the 660-nm LED (intensity of 0.04 mW/cm^2). We plotted the ratio of current under illumination to dark current (I_{light}/I_{dark}) in Figure 5. It is clear that the enhancement of current upon illumination is far greater for LMS ($I_{light}/I_{dark} \approx 2300$ at $V = 0$), where the excitons are trapped at the interface with PEDOT:PSS, than for SML ($I_{light}/I_{dark} \approx 73$ at $V = 0$), where the excitons are trapped away from the interface. As expected, the ratio I_{light}/I_{dark} for LMS drops off precipitously for V more negative than V_{OC} (at which point, the current begins to flow in the opposite direction: from EGaIn to ITO). The ratio I_{light}/I_{dark} for LMS also decays as V is increased from 0 in the positive direction. This result indicates that I_{dark} has a much steeper dependence on the applied electric field than the photocurrent (I_{PC}), since $I_{light}/I_{dark} = (I_{PC} + I_{dark})/I_{dark}$, and an increase in I_{dark} (with increasing V) without a concomitant increase in I_{PC} would decrease the ratio I_{light}/I_{dark}. We will show later that the values of V we apply are probably not large enough to ionize excitons in the QDs (away from the interface with PEDOT:PSS); rather, the applied electric field either (i) increases the yield of separation of charge at the interface with PEDOT:PSS, (ii) increases the rate of electron transport through the array (from PEDOT:PSS to EGaIn), or (iii) increases the rate of electron transfer from the QDs to EGaIn. Further study is needed to clarify the dependence of photocurrent on the applied electric field.

Photocurrent Action Spectra. The photocurrent action (PCA) spectrum is a final test of our hypothesis that, at $V = 0$, it is only excitons that can reach the interface between the QDs and PEDOT:PSS that contribute to the photocurrent. The PCA spectrum—a plot of photocurrent as a function of wavelength of excitation—reveals which excited states produce charge carriers in junctions that contain multiple chromophores with different absorption spectra. The peaks in the PCA spectrum should match the absorbance features of those QDs whose excitons either separated into charge carriers that contributed to the observed photocurrent or traveled to other QDs, where they separated into charge carriers. We recorded PCA spectra of the junctions LLL, LMS, and SML. Figure 6 shows the absorption spectra of the S, M, and L QDs (left y-axis) and the PCA spectra (right y-axis). The PCA spectra show the normalized photocurrent ($I_{light} - I_{dark}$) at $V = 0$ as a function of excitation wavelength. Our tunable excitation source for this experiment was a SPEX Fluoromax-3 spectrophotometer with a 450-W Hg−Xe arc lamp in combination with a monochromator (intensity = 38 μW/cm^2).

As expected, the PCA spectrum for LLL closely matched the absorbance spectrum of the L QDs. The PCA spectrum for LMS matched the combined absorbance spectra of its component QDs. (We will discuss this result below, in the context of energy transfer.) The key piece of evidence is the PCA spectrum of SML. This PCA spectrum only mirrors the absorbance

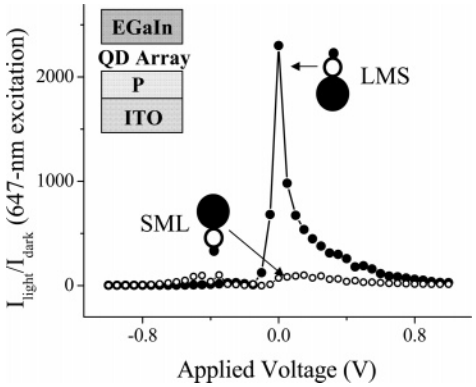

Figure 5. Ratio of current under illumination (I_{light}) to dark current (I_{dark}) as a function of voltage for the junctions ITO/PEDOT:PSS/**X**/EGaIn, **X** = SML and LMS. The excitation source was the 647 nm line of an Ar-ion laser (intensity = 10 mW/cm^2).

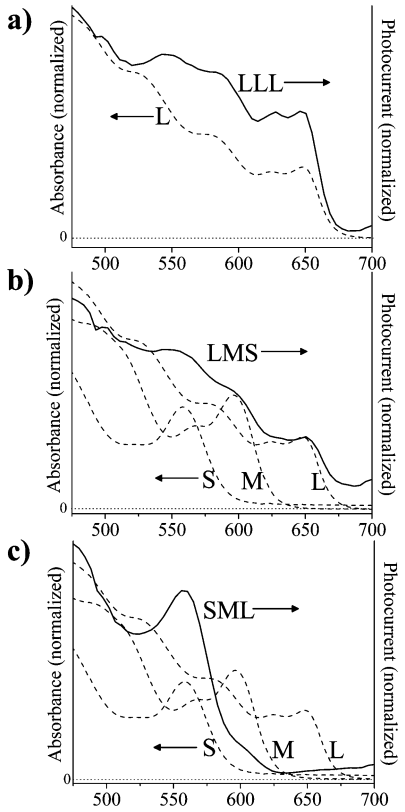

Figure 6. Photocurrent action (PCA) spectra (normalized photocurrent as a function of excitation wavelength, solid lines, right axes) for the junctions ITO/PEDOT:PSS/**X**/ EGaIn, **X** = LLL (a), LMS (b), and SML (c). The tunable excitation source for these spectra was a 450 W Hg−Xe arc lamp in combination with a monochromator (intensity = 38 μW/cm^2). Also shown with each PCA spectrum are the ground-state absorbance spectra for films of the S, M, and L QDs on glass (dashed lines, left axes).

features of the S QDs, which are the QDs at the interface with PEDOT:PSS. In this junction, excited states in the L and M QDs (created at excitation energies lower than E_g for the S QDs) cannot migrate to the S QDs at the interface. This spectrum therefore shows that it is *only* excited states at the interface between the QDs and PEDOT:PSS that contribute to the photocurrent.

Proposed Mechanism for Generation of Photocurrent. In light of the evidence in the preceding section, we propose a mechanism for the generation of photocurrent (Figure 7): Upon formation of the junction (at $V = 0$), thermal equilibration of the population of electrons in the ITO and the EGaIn (which have a difference in work function of ∼0.7 eV) occurs—that is, electrons move from the EGaIn to the ITO via the external circuit until the Fermi levels of the two electrodes are at equal energies. This equilibration results in negative charging of the surface of ITO (which increases its effective Fermi level by 0.35 eV) and positive charging of the surface of EGaIn (which decreases its effective Fermi level by 0.35 eV) (see Figure S5 for equilibrated energy level diagrams). An electric field, E, therefore exists across the junction at zero applied bias. If we assume that this field drops entirely across the layers of QDs (and not at all across the "metallic" layer of PEDOT:PSS[49]), then the field ($E = V/L$, where $L = 80$ nm) present across the array is 8.8×10^4 V/cm.

When photoexcitation of the QDs creates an electron−hole pair in a QD near the interface with PEDOT:PSS, PEDOT:PSS accepts a hole from (donates an electron to) the singly occupied HOMO of the photoexcited QD. The QD adjacent to the PEDOT:PSS is now negatively charged. The electric field (due to the difference in work functions between the electrodes) pushes the electron in what is now the singly occupied HOMO of the QD anion toward the EGaIn electrode via the LUMOs of neutral QDs (whose excited states have decayed or moved to other QDs), and eventually across the interface between the QDs and EGaIn. This process results in net *electron transport* from ITO to EGaIn and yields a positive ($I > 0$) photocurrent.[50] In this mechanism, the current originates from photoexcited electrons and holes in the layers of QDs near the interface with PEDOT:PSS.

Why do electrons separate only at the interface with PEDOT:PSS, and not (i) at the interface between the QDs and EGaIn or (ii) in the layers of QDs? A model developed to fit the magnitude of photocurrent as a function of applied field in junctions containing arrays of CdSe QDs (with diameters of ∼3−6 nm) yielded an energy of ∼150 meV required to split an exciton—that is, to overcome the Coulomb binding energy of the electron−hole pair and the tunneling barrier imposed by the organic capping groups—in order to transfer the electron (or hole) from the QD to a neighboring QD or to a neighboring polymer or electrode.[28] The interface between the QDs and PEDOT:PSS is a "type-II heterojunction"—that is, the VB of PEDOT:PSS is positioned (energetically) between the HOMO and LUMO of the QDs, and the CB of PEDOT:PSS is positioned above both the HOMO and LUMO of the QDs.[51] The practical implication of this "staggered" configuration of energy levels is that PEDOT:PSS can accept a hole from the excited state of the QD in an exothermic ($|\Delta G| > 1$ eV) hole transfer (or, if the PEDOT:PSS were excited, a QD could accept an electron from the excited state of PEDOT:PSS in an

(49) Menon, R. *Handbook of Conducting Polymers*; Marcel Dekker, Inc.: New York, 1998.

(50) Electron transport through the array LMS, which involves electron transfer from L QDs to M QDs and from M QDs to S QDs, is an energetically uphill process (both electron transfers have $\Delta G \approx 100$ meV, ∼2.3 kcal/mol, ∼4kT). If we assume that the electric field across the array at zero bias (8.8×10^4 V/cm) drops evenly across the array, then the energy available from this field is <10 meV for both electron transfers, less than is required. This number (8.8×10^4 V/cm) does not, however, take into account the additional electric field created as charges continuously separate at the PEDOT:PSS/QD interface to create QD anions at this interface. We believe that it is this build-up of negative charge in the QDs near the PEDOT:PSS that supplements the electric field created by the difference in work functions of the electrodes and pushes the electrons across the QD array and into the EGaIn.

(51) Shik, A.; Bakueva, L.; Ruda, H. E. *Phys. Stat. Solidi B* **2005**, *242*, 1183.

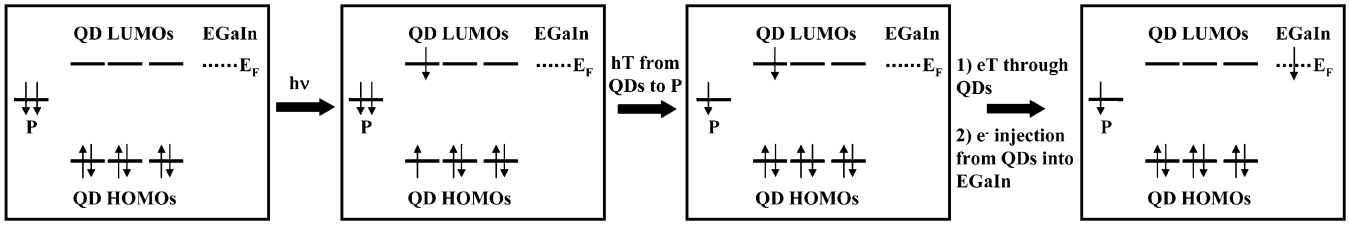

Figure 7. Proposed mechanism for the generation of photocurrent in the ITO/P /QD/EGaIn junctions (where the energies of the frontier orbitals of the QDs are drawn as constant throughout the array, for simplicity). (i) Half-filled HOMOs of photoexcited QDs adjacent to PEDOT:PSS donate holes to the VB of PEDOT:PSS. (ii) The electric field resulting from equilibration of EGaIn and ITO electrodes through the external circuit pushes electrons through the LUMOs of the QDs toward the EGaIn, and through the interface between the QDs and EGaIn. (The dotted lines indicate an approximate value of the Fermi energy of EGaIn, E_F, after this equilibration.) In this diagram, P ≡ PEDOT:PSS, $h\nu$ ≡ photoexcitation of the QDs, eT ≡ electron transfer, and hT ≡ hole transfer.

exothermic electron transfer). This exothermicity provides enough driving force to split the exciton at the interface between the two materials.

In order for an exciton to split at the interface between EGaIn and the QDs (option (i)), electron transfer must occur from the LUMO of the photoexcited QD to EGaIn. This process has little or no driving force: even after equilibration with ITO, the Fermi level of EGaIn is approximately energetically degenerate with (or slightly higher in energy than) the LUMOs of the QDs. Separation of charge before the exciton recombines (which occurs in ∼10 ns[28]) at this interface is therefore improbable.

In order for mobile electrons and holes to be created within the layer of QDs—that is, for option (ii) to occur—the electric field due to the mismatch between the work functions of ITO and EGaIn (at $V = 0$) must be large enough to separate the electron−hole pairs created by photoexcitation of the QDs (i.e., to move an electron from one particle to its nearest neighbor over a distance equal to the center-to-center distance between two QDs in the array).[28] The field available to split an exciton in *our* arrays is the fraction of the total field (8.8×10^4 V/cm) that drops over this distance (10 nm for L QDs, 5.5 nm for M QDs, and 4.4 nm for S QDs, including the 0.2-nm separation between QDs). If we assume that the field drops uniformly across the array of QDs, then this fraction is 1.1×10^4 V/cm (L QDs), 6.0×10^3 V/cm (M QDs), and 4.8×10^3 V/cm (S QDs). The energy available to split an exciton in each of these systems (the electric field × center-to-center distance) at $V = 0$ is then 11 meV (L QDs), 3.3 meV (M QDs), and 2.1 meV (S QDs). These energies are all less than a factor of 10 smaller than the energy necessary to ionize an exciton (150 meV). In fact, exciton ionization would probably not occur even at the highest values of V we applied ($V = 2.0$ V); the energies available at this bias are smaller than 150 meV by at least a factor of 5 (for all of the sizes of QDs).

It is possible that electrons and holes separate at the interfaces between the S QDs and the M QDs, and between the M QDs and the L QDs, where the offset in the energy of the LUMOs (∼100 meV) is on the same order as the energy required to split the exciton (150 meV). This mechanism may, in fact, account for the small photocurrent produced upon excitation at ∼600 nm (the absorbance of the M QDs) in the PCA spectrum of the SML array (Figure 6c). The dramatically larger photocurrent produced when QDs near the interface with PEDOT:PSS are excited (Figures 5 and 6c), however, shows that charge separation at this interface dominates the production of photocurrent over that at interfaces between different sizes of QDs.

Do Excitons Created away from the Interface between the QDs and PEDOT:PSS Contribute to the Photocurrent via Energy Transfer? Fluorescence quenching experiments have shown that the rate of resonant energy transfer in CdSe QD arrays is at least 10^8 s^{-1}, and that QDs will transfer energy to other QDs with larger diameters.[5] Inspection of the PCA spectrum is a straightforward way to determine whether excitons created at a distance from the interface between the QDs and PEDOT:PSS migrate to the interface and charge-separate to contribute to the photocurrent. If we assume that, as we have shown, separation of charge occurs at this interface at 0 V, then the fact that the PCA spectrum (recorded at 0 V) for LMS matched the combined absorbance spectra of its component QDs (Figure 6) means that excitons in all three layers of QDs migrated to the QDs with the lowest-energy excited state (the L QDs) and separated into charge carriers that contributed to the photocurrent.[52] This result implies that, within a solar cell or photodetector, even if separation of electrons and holes can only occur at an interface with an electrode or a complementary active material, energy absorbed by QDs away from this interface will not be wasted but rather funneled to this interface to contribute to the photocurrent.

Open-Circuit Voltage in the Dark and under Illumination (Photovoltage). The open-circuit voltage, V_{OC}, is that at which $I = 0$—that is, at $V = V_{OC}$, there is net zero current flowing through the device. For samples in which the QDs next to the PEDOT:PSS are photoexcited, at V_{OC}, the rate of transfer of photoexcited electrons from the LUMOs of the QDs to the VB of PEDOT:PSS equals the rate of electron transfer from the VB of PEDOT:PSS to the half-filled HOMOs of the photoexcited QDs. Table 2 gives the values of V_{OC} for the QD junctions measured in the dark and when excited by LEDs at 565 and 660 nm.[53] We extracted values for V_{OC} by scanning V from 0 → 0.5 → −1.0 → 0 V in steps of 0.05 V, connecting the points by straight-line segments, and determining the value of V at which the interpolated $I-V$ plots crossed 0 A.

(52) Our values for EQE present conflicting evidence as to whether excitons created away from the interface also contribute to the photocurrent. We believe, however, that using the EQEs—which depend on the rates of numerous processes whose description is beyond the scope of this work—to address the question of energy transfer would be over-interpretation (especially considering that the uncertainties of the EQEs make them indistinguishable from one another in many cases).

(53) In the dark, current probably results from the transfer of thermally excited electrons in the PEDOT:PSS to the LUMOs of the QDs, because the bandgap of PEDOT:PSS ($E_g = 1.6$ eV) is smaller than that of the QDs ($E_g = 1.9$ eV), so its conduction band is more populated than the LUMOs of the QDs at room temperature.

Table 2. Open Circuit Voltage (V_{OC}) of the Junctions ITO/P/**X**/EGaIn in the Dark and under Illumination (with Excitation from LEDs at 565 and 660 nm)

	V_{OC} (V)[a]		
X	dark	565 nm	660 nm
LLL	-0.06 ± 0.02[b]	-0.12 ± 0.03	-0.09 ± 0.02
LMS	-0.06 ± 0.03[b]	-0.17 ± 0.01	-0.07 ± 0.04
MMM	-0.51 ± 0.14[b]	-0.52 ± 0.04	-0.57 ± 0.15[b]
SML	-0.64 ± 0.14[b]	-0.56 ± 0.03	-0.48 ± 0.10[b]
SSS	-0.66 ± 0.14[b]	-0.69 ± 0.14	-0.61 ± 0.13[b]

[a] V_{OC} is presented as a mean ± standard deviation of between 14 and 21 values (depending on **X**). [b] These traces were hysteretic; V_{OC} was taken from the segment $-V \rightarrow 0$, after the junction discharged under negative bias (see the text for further explanation).

When there were no photoexcited QDs at the interface between the QDs and PEDOT:PSS—that is, for all junctions in the dark, and for **X** = MMM, SML, and SSS under excitation at 660 nm—charge accumulated in the junctions during the portion of the scan from $V = 0 \rightarrow 0.5 \rightarrow 0$, probably because electrons injected into the PEDOT:PSS from the ITO became trapped in the polymer. This charging resulted in a hysteretic $I-V$ trace: V_{OC} was different during the portion of the scan from $0 \rightarrow -1.0$ V (when the junction became charged) than during the portion from -1.0 V $\rightarrow 0$ (when the junction discharged). For those junctions whose traces were hysteretic, the values of V_{OC} in Table 2 were therefore taken from the portion of the scan from -1.0 V $\rightarrow 0$ (after the junction had discharged).

For all junctions and wavelengths, (i) V_{OC} was similar in the dark and under illumination, and (ii) V_{OC}(L**X**) < V_{OC}(M**X**) < $\sim V_{OC}$(S**X**), so it appears that V_{OC} is dictated by the size of the QDs at the interface between the QDs and PEDOT:PSS. These results are reasonable, considering that V_{OC} is the *net* energy gained by an electron upon being excited from its ground state and traveling from its point of origin into the EGaIn electrode. According to our mechanism for photocurrent, (i) an electron gains energy, E_g ($\approx E_{LUMO} - E_{HOMO}$ of the QD), via photoexcitation, and (ii) the excited state of the QD at the interface between the QDs and PEDOT:PSS is quenched by donation of an electron from the VB of PEDOT:PSS (which came from ITO) to the half-filled HOMO of the QD. This charge-transfer process subtracts an energy E_F(ITO) $- E_{HOMO}$(QD) from E_g (where E_F(ITO) is the Fermi level of ITO). The *net* energy gained by the electron is therefore E_{LUMO}(QD) $- E_F$(ITO). This difference increases as the diameter of the QD decreases;[1] we would therefore predict V_{OC}(L**X**) < V_{OC}(M**X**) < V_{OC}(S**X**), which is approximately what we observe.

Conclusions

We measured the current produced by junctions incorporating arrays of colloidal CdSe QDs of a single size and of multiple sizes, with ITO-PEDOT:PSS and eutectic Ga/In (EGaIn) electrodes (Figure 1), when these junctions were excited with various wavelengths of light. In the junctions containing multiple sizes of QDs, we could localize the photoexcitation in different parts of the junction (i.e., near the interface between the QDs and either PEDOT:PSS or EGaIn) by using light that was absorbed primarily by only one of the three sizes of QDs.

Size-Selective Photoexcitation as an Analytical Tool. Our work suggests that, by constructing multiple junctions that have effectively indistinguishable absorption spectra but a different spatial arrangement of QDs, one can determine how the location of a particular QD within the array—that is, its proximity to an electrode, a complementary active material, or another QD of a different size—affects the contribution of its excited state to the observed photocurrent. Specifically, size-selective excitation in junctions incorporating multiple sizes of QDs allowed us to answer the following three questions:

(i) *What is the location of the interface at which photoinduced charge separation (to create electrons and holes from excitons) occurred?* We determined conclusively that, at $V = 0$ V, separation of charge at the interface between the QDs and PEDOT:PSS dominated the production of photocurrent (Figures 4b, 5, and 6). We believe that this mechanism dominated over the majority of the range of V we examined—$V = 0 \rightarrow +1$ V (for behavior of the junctions when $V < 0$, please see a separate publication[1])—but we did not determine the value of V at which other mechanisms (hole conduction induced by separation of charge at the interface between the QDs and EGaIn, and ionization of excitons within the array of QDs) began to contribute.

(ii) *Does the energy absorbed by the QDs redistribute before separation of charge?* The photocurrent action (PCA) spectra (Figure 6) of the junctions containing multiple sizes of QDs indicated that, when energetically favorable, excitons created away from the interface between the QDs and PEDOT:PSS traveled to this interface and split to create charge carriers. The inspection of the PCA spectra is a much more direct way to determine how energy is redistributed in the junction than is comparison of external quantum efficiencies (EQEs) (Table 1) between junctions. For instance, one would expect the EQE of LMS to be approximately 3 times that of SML with excitation at 565 nm, because excited states in all three layers are contributing to the photocurrent in LMS, while only excited states in the layer of S QDs are contributing to the photocurrent in SML. In fact, $EQE(LMS)_{565}$ is only a factor of $\sim$1.4 greater than $EQE(SML)_{565}$ (Table 1 and Figure 4b), but this result may be attributed to several factors, including different rates of charge transfer across the interface between the QDs and PEDOT:PSS or between the QDs and EGaIn, or a different density of sites that trap charge in the two junctions (due to slight variation in conditions used to prepare or deposit the QDs). Both of these factors would affect the current through the device but are independent of the tendency of energy to redistribute through the array prior to separation of charge.

(iii) *How does the magnitude of the photovoltage depend on the locations of various sizes of QDs within the junction?* The magnitude of the photovoltage (V_{OC} under illumination) increased as the size of the QDs—and the gap between the energies of the LUMOs of the QDs and the valence band of PEDOT:PSS—at the interface between the QDs and PEDOT:PSS decreased (Table 2). The photovoltage therefore appears to be proportional to the difference between the energy absorbed when an electron is promoted from the HOMO of the QD to the LUMO of the QD and the energy lost when an electron is transferred from the valence band of PEDOT:PSS to the half-filled HOMO of the QD. This result supports our hypothesis that photocurrent is generated by charge transfer at the interface between the QDs and PEDOT:PSS.

The method of localizing excitation in an array of QDs of multiple sizes in order to identify the interface for separation

of charge would be useful in analysis of a solar cell composed of QDs plus a *p*-type material (a heterojunction cell). Ideally, in a heterojunction cell, excitons migrate to the interface between the *n*-type and *p*-type materials and separate into electrons and holes. Use of localized excitation would determine whether another unfavorable process—for example, separation of charge at the interface between QDs and an electrode—were taking place, in which case a layer of a material that blocks the passage of electrons or holes might be incorporated between the QDs and the electrodes to stop the unproductive quenching process.

Applications for Arrays of Multiples Sizes of QDs in Photonic Devices. The incorporation of an array of multiple sizes of QDs as an active material in zero-bias devices like solar cells and photodetectors presents several potential advantages: (i) The gradient in potential formed from the gradient in size can, as we have shown, funnel energy to the interface where separation of charge occurs. (ii) The gradient in potential could possibly funnel electrons and holes (through a series of exothermic charge transfers) from the interface, where they separate from each other, to the collecting electrodes. This vectorial charge transfer might, in part, offset the low mobility of electrons and holes in arrays of QDs (relative to that in bulk semiconductors) by providing a greater intrinsic electric field than exists due to the difference in work functions of the electrodes. (iii) Heterojunction devices with arrays with one size of QDs contacting the collecting electrode and another size of QDs contacting the complementary active material provide a means of achieving energetic resonance at both contacts for efficient separation and collection of charge.

A final interesting application of the array of multiple sizes of QDs is vectorial transport of charge (from the electrodes where charge is injected to the interface where charges combine and emission occurs) in a light-emitting diode. One possible architecture is combination of an array of CdTe QDs (which is *p*-type) with an array of CdSe QDs (which is *n*-type), where both arrays have a gradient of sizes of QDs (the smallest QDs adjacent to the electrodes and the largest adjacent to the emitting layer at the center of the device).

Acknowledgment. We acknowledge funding from NSF CHE-0518055 (Harvard), the NSEC Program of the National Science Foundation, award no. PHY-0117795 (MIT), and the U.S. Army through the Institute for Soldier Nanotechnologies, under contract no. DAAD-19-02-0002 with the U.S. Army Research Office (MIT). The authors used the shared facilities supported by the National Science Foundation under NSEC (PHY-0117795 and PHY-0646094, Harvard), MRSEC (DMR-0213805, Harvard), and MRSEC (DMR 0213282, MIT). E.A.W. thanks the Petroleum Research Fund of the American Chemical Society for a fellowship (PRF no. 43083-AEF). V.J.P. was funded in part by the NSF MRSEC program (DMR 0213282) at MIT. The authors thank E. Lavoise for preparing the samples for TEM.

Supporting Information Available: Experimental details, error analysis, and Figures S1−S5, showing additional absorption spectra of the QDs, atomic force micrographs of the QD films, a schematic diagram of the procedure used to make the TEM samples, and an energy level diagram of the connected device. This material is available free of charge via the Internet at http://pubs.acs.org.

JA076439+